Particle-in-cell simulation of collisionless undriven reconnection with open boundaries

Alex Klimas, Michael Hesse, and Seiji Zenitani

Related Articles

Simulation of relativistically colliding laser-generated electron flows
Phys. Plasmas 19, 113110 (2012)

On the breaking of a plasma wave in a thermal plasma. I. The structure of the density singularity
Phys. Plasmas 19, 113102 (2012)

Upper limit power for self-guided propagation of intense lasers in plasma
Appl. Phys. Lett. 101, 184104 (2012)

THz emission control by tuning density profiles of neutral gas targets during intense laser-gas interaction
Appl. Phys. Lett. 101, 181113 (2012)

Ionization effects in the generation of wake-fields by ultra-high contrast femtosecond laser pulses in argon gas
Phys. Plasmas 19, 103104 (2012)

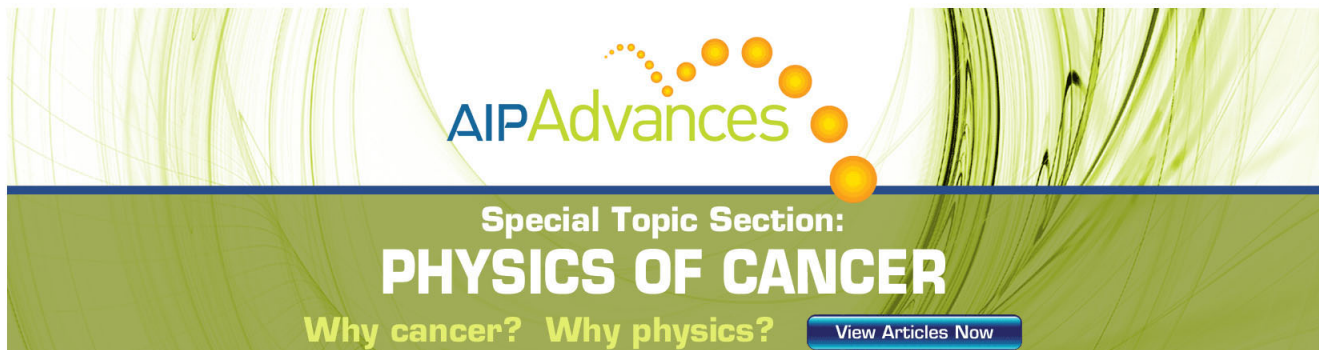## Additional information on Phys. Plasmas

Journal Homepage: http://pop.aip.org/

Journal Information: http://pop.aip.org/about/about_the_journal

Top downloads: http://pop.aip.org/features/most_downloaded

Information for Authors: http://pop.aip.org/authors

Particle-in-cell simulation of collisionless undriven reconnection with open boundaries

Alex Klimas,[1,2] Michael Hesse,[3] and Seiji Zenitani[4]

[1]*GPHI at University of Maryland, Baltimore County, Baltimore, Maryland 21228, USA*
[2]*Emeritus at NASA Goddard Space Flight Center, Greenbelt, Maryland 20771, USA*
[3]*NASA Goddard Space Flight Center, Greenbelt, Maryland 20771, USA*
[4]*National Astronomical Observatory of Japan, 2–21-1 Osawa, Mitaka, Tokyo 181–8588, Japan*

The results are discussed of a $2\frac{1}{2}$ dimensional, undriven, fully open-boundary particle-in-cell simulation of symmetric, anti-parallel reconnection. It is shown that the reconnection rate as measured by the strength of the out-of-plane electric field component at the dominant x-line is fast and unrelated to the emergence of magnetic islands. In contrast, it is shown that this reconnection rate normalized by the inflowing $V_{Alf,in}B_{in}$ at the x-line does show a striking relationship to island emergence in a majority of cases. A detailed study of an outflow jet is discussed. It is shown that for this example the concept of an outer electron diffusion region is a misnomer. In this jet, the electrons are tied to the magnetic field motion in the local Hall plane. The extended electron diffusion region (E^2DR) surrounding a reconnection site, where the out-of-plane non-ideal electric field is greater than zero, is discussed. The width d of this region is shown to remain between the ion and electron bounce length scales, in contrast, to the behavior in driven reconnection simulations in which d evolves from the electron bounce width to the ion bounce width, where it remains. The boundaries of the E^2DR in the outflow directions are shown to mark the positions at which the electrons are magnetized and begin their drift with the field in the local Hall plane. It is shown that the aspect ratio d/L, in which L is the length of the E^2DR, yields an excellent approximation to the normalized reconnection rate while the expression T_i/L, in which T_i is the ion temperature at the x-line, yields an excellent approximation to the un-normalized rate. It is concluded that the dynamics of the electrons in the E^2DR is intimately related to the reconnection rate and it is suggested that in two dimensional, anti parallel, symmetric simulations, this region is the correct choice for the controversial electron diffusion region. © *2012 American Institute of Physics*. [http://dx.doi.org/10.1063/1.3699032]

I. INTRODUCTION

The role of the electron diffusion region (EDR) in collisionless magnetic reconnection remains a central and unresolved issue. One of the primary and most challenging goals of NASA's upcoming Magnetospheric Multiscale mission (http://mms.space.swri.edu/index.html) will be to detect and examine the properties of this small spatial region where it occurs in Earth's magnetosphere. At present, however, even a generally accepted definition of the EDR is not available. Much of the controversy surrounding this definition has arisen recently with the advent of open-boundary techniques for particle-in-cell (PIC) reconnection simulations.[1–12]

For two dimensional simulations, assuming that the y-direction is the out-of-plane direction, a straightforward definition of the EDR could be that region, associated with a reconnection site, in which $E'_y = E_y + [\mathbf{v_e} \times \mathbf{B}]_y \neq 0$; i.e., that region in which the out-of-plane electric field is non-ideal, and the electrons are not frozen to the in-plane motion of the magnetic field.

Daughton *et al.*[4] have studied the dimensions of this region ($E'_y \neq 0$) using fully electromagnetic, $2\frac{1}{2}$ dimensional, open-boundary, PIC reconnection simulations. As a consequence of the open-boundary conditions, they were able to extend their simulations to times greater than had

been possible before. They showed that as time increased so did the length in the outflow directions of the $E'_y \neq 0$ region, increasing to tens of ion inertial lengths. Simultaneously, the lengths of the electron outflow jets and the out-of-plane electron current sheet grew as well, while the reconnection rate decreased as these lengths increased. This process went on until a magnetic island formed that divided this region, temporarily allowing the reconnection rate to recover and beginning the lengthening process once again. Thus, Daughton *et al.* concluded that the increasing length produced a bottle neck for the electron flow that limited the reconnection rate. They also noted that the length of this region tended to grow well beyond that of the region of relatively uniform electron inflow, which, they argued, should provide a measure of the EDR length. As a proxy for measuring this length, they chose the separation of the electron outflow velocity maxima. With this choice, they were able to construct an upper bound for the reconnection rate that agreed nicely with the results of their simulations. They concluded that the EDR is that portion of the $E'_y \neq 0$ region lying between the maxima in the electron outflow velocities, with length significantly smaller than that of the entire region. They further concluded that the electrons control the reconnection rate due to the lengthening of the EDR, as they defined it.

19, 042901-1

Karimabadi *et al.*[7] later refined the EDR description given in the preceding paragraph. Analyzing results obtained using the same open-boundary simulation code, they concluded that the EDR is the entire region defined by $E'_y \neq 0$ but they divided this region into inner and outer parts. In this view, the inner portion consists of the entire EDR, as it was defined by Daughton *et al.*[4] while the outer regions contain the remainder of the region of $E'_y \neq 0$. Over most of the inner region they found $E'_y > 0$, indicating that the electrons lag behind the in-plane magnetic field motion, while in the outer portions they found $E'_y < 0$, indicating that the electrons are outrunning the field in these outflow regions, in the so called super-Alfvénic outflow jets.[13,14] They concluded that the outer boundaries of the outer regions are at the positions where the electrons finally become magnetized, coinciding with the ends of the extended outflow jets. Overall, in this picture, the EDR consists of a region, a few electron inertial lengths thick and tens of ion inertial lengths long. In contrast to the results of Daughton *et al.*, the reconnection rates obtained in this study consisted of intervals of fast, relatively steady reconnection plus intervals containing strong fluctuations when magnetic islands formed. Karimabadi *et al.* argued that the competing factors that control the elongation of the EDR can come into balance, resulting in continuous reconnection sometimes but not necessarily always. Although considerably further developed, this theory of the EDR still concludes that it is the electron dynamics of the EDR that controls the reconnection rate.

Shay *et al.*[13] have studied the structure of the EDR employing a series of PIC simulations of various mass ratios and simulation domain sizes. These were closed, periodic simulations but on large computational domains such that in each case fully developed, steady reconnection was achieved before the boundary conditions could affect the plasma at the x-line. (Note: Shay *et al.* use the term, electron dissipation region, to describe the EDR, as defined by Daughton *et al.*[4] and Karimabadi *et al.*[7] However, more recently Zenitani *et al.*[15,16] have introduced a formal definition of the electron dissipation region, D_e, that differs from that of the EDR. To avoid confusion in this discussion, we will use the term EDR while, even so, describing the Shay *et al.* results.) Shay *et al.* found dissimilar behavior for the out-of-plane electron current sheet and the extended EDR. The length of the current sheet saturated as each of the simulations proceeded with a mass ratio dependence that implied the current sheet length would be ≈ 1 ion inertial length for the true mass ratio. The lengths of the electron outflow jets grew continuously to 10s of ion inertial lengths right up to the ends of their simulations. Despite this stretching of the outflow jets and the absence of magnetic island formation, they achieved steady reconnection rates that were in agreement across the series of simulations, in contrast, to Daughton *et al.*[4] This result, plus the related saturation of the current sheet lengths, implied that the electron dynamics of the EDR did not control the reconnection rate. In agreement with Karimabadi *et al.*,[7] however, they did find a two-scale structure of the EDR with an inner region defined somewhat differently but essentially the same outer region containing the super-Alfvénic electron outflow jet in which the electrons are decoupled from and outrunning the magnetic field.

Hesse *et al.*,[17] however, have thrown the super-Alfvénic outflow jet concept into doubt. They noted that the presence of the out-of-plane Hall quadrupole magnetic field implies that in the neighborhood of the neutral sheet, the magnetic field lines lie in a plane rotated with respect to the 2-D (x, z) simulation plane. Thus, they examined the properties of the outflow jet in a coordinate system that is rotated about the z axis, so that the field lines lie in the (x', z) plane, the "local Hall plane," in the neighborhood of the neutral sheet; i.e., near the neutral sheet $B_{y'} = 0$. (see Fig. 2 of Zenitani *et al.*[15] for an illustration of the rotated field lines) Hesse *et al.* found the surprising result that in this rotated coordinate system, at a position within the outflow jet, the electric field component $E_{y'}$ and the electron convection electric field component $E_{cy'} = -[\mathbf{v}_e \times \mathbf{B}]_{y'}$ were almost equal, implying that the electrons drift with the in-Hall-plane field line motion and that $E'_{y'} \approx 0$. At least at the position within the outflow jet that they examined, this result is inconsistent with the assumption of a super-Alfvénic outflow jet in which the electrons are outrunning the field line motion. Hesse *et al.* also found that the magnetic field reversal in the outflow jet is supported by a diamagnetic current sheet directed orthogonal to the local Hall plane and carried by the electrons. It is the projection of the high electron velocity in this current sheet onto the simulation plane that gives the appearance of a super-Alfvénic outflow jet.

Klimas *et al.*,[12] studying the results of a 2½ dimension, fully open-boundary, driven PIC reconnection simulation, have introduced a definition of the EDR that is consistent with the Hesse *et al.*[17] results. In this definition, the EDR is that region surrounding the x-line in which $E'_y > 0$; the outer EDR, $E'_y < 0$, is not included. Since this definition was shown to exhibit extended regions in both the inertial and the thermal contributions to E'_y that had not been included previously, this region was named the extended electron diffusion region (E²DR). In a coordinate system, in which the outflow and inflow directions are in the x and z directions, respectively, turning points in the outflow directions were defined as those positions on either side of the x-line where the Larmor radius in B_z equals the distance to the x-line (analogous to a bounce-width calculation in the orthogonal direction).
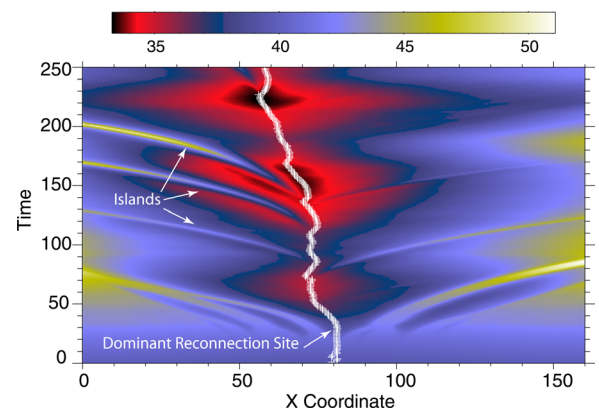

FIG. 1. Evolution with time in units of Ω_i^{-1} of a cut through the flux surface in the *x*-direction at the *z*-position of the x-line. The emergence and propagation of magnetic islands is shown. The path taken by the dominant x-line is indicated by the white crosses.
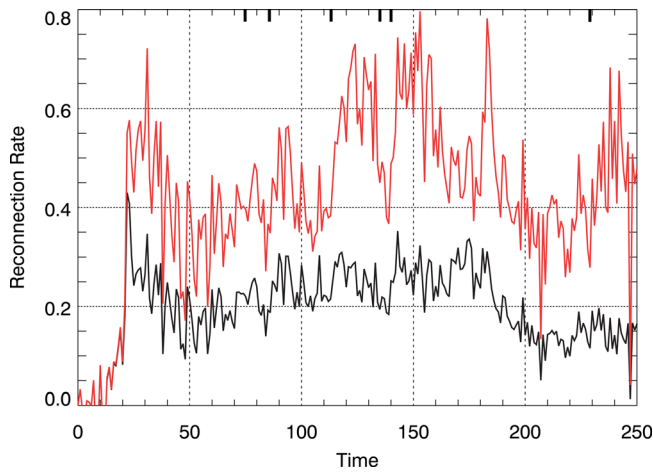
FIG. 2. Black: the reconnection rate as measured by the strength of the out-of-plane electric field component at the position of the dominant x-line. Red (gray): reconnection rate normalized by $V_{A,in}B_{in}$. Vertical bars at top of figure show the approximate times at which magnetic islands appeared.

These turning points were found to lie just inside the boundaries of the E²DR, indicating that the outflow boundaries of the E²DR mark the positions where the electrons become magnetized in the outflow jet B_z and leading Klimas *et al.* to speculate that the outer boundaries of the E²DR mark the inner boundaries of the regions in which the results of Hesse *et al.*[17] apply. The widths, in the z direction, of both the thermal and the inertial contributions to the E²DR were found to extend to the ion bounce width over the entire simulation following the initial transient period. However, the extensions of these contributions were found to cancel out for the first 150 Ω_i^{-1} ($\Omega_i^{-1} =$ ion Larmor period in the asymptotic magnetic field strength) so that the E²DR width remained at the electron bounce width during this period.[3] Later, however, this cancellation failed, with the inertial contribution dominating and the width of the E²DR grew to, and remained at the ion bounce width. The length of the E²DR was found to fluctuate about a relatively constant value with isolated deep temporary reductions at the times of island formation. No consistent signatures of these reductions were found in the reconnection rate, which fluctuated on short and long timescales about the strength of the driving field strength in this driven simulation. Klimas *et al.* did not offer an opinion on whether the electrons controlled the reconnection rate but they did present two examples in which the dimensions of the E²DR could be used to produce quite accurate detailed fits to the evolution of the reconnection rate over the entire simulation. On this basis, plus the restrictions presented by Hesse *et al.*, they concluded that it is the E²DR, rather than any of the other EDR definitions discussed above, that is relevant to further investigations of the electron role in reconnection.

In this paper, we move to a closer comparison to the simulations of Daughton *et al.*[4] and Karimabadi *et al.*[7] by discussing the results of an undriven version of the simulation of Klimas *et al.*[12] Compared to the simulation setup of Klimas *et al.*, two important changes have been made: First in this undriven simulation, a zero-gradient boundary condition has been applied to E_y at the inflow boundaries; the

value of E_y has been allowed to float but in a manner that ensured that the x-line remained approximately centered in the z-direction. An explanation is given below. Second, to alleviate the problem that Klimas *et al.* had with declining particle density on their simulation grid, a separate source of particles has been introduced at the inflow boundaries to maintain the inflow density at a predetermined value. Other changes are minor and are discussed in the Appendix.

We have examined the dimensions of the E²DR over the course of this undriven simulation. As in the driven run, we find that the boundaries of the E²DR in the outflow directions lie just outside the turning points. Surprisingly, we find the width of the E²DR lies between the electron and ion bounce widths over the entire simulation following a brief transient period. Because in the driven run of Klimas *et al.*,[12] the widths of the thermal and inertial contributions to the E²DR were very close to the ion bounce width, it was impossible to decide if the E²DR width was an independent electron property or simply a reflection of the ion dynamics. In this undriven simulation, it appears clear that the E²DR width is a property of the electron dynamics. This result is of particular importance, since we continue to find that, if R_A is the aspect ratio of the E²DR, then R_A gives an accurate fit to the reconnection rate, normalized by the inflowing $V_{alf,in}B_{in}$ at the dominant x-line, over the entire simulation, again following the initial transient period. Further, if T_i is the ion temperature and L is the length of the E²DR, we also find that T_i/L yields a similarly accurate fit to the un-normalized reconnection rate. It should be noted that for this simulation, we have deliberately maintained the density at the inflow boundaries higher than the initial background density. Consequently, when the inflowing plasma reaches the x-line several of the plasma properties change relatively quickly including the reconnection rate, which drops precipitously to a new approximately steady value. Both of the fits to the reconnection rate, R_A and T_i/L, follow this rapid transition faithfully.

There are intervals in this simulation during which multiple magnetic islands are formed and propagate to the outflow boundaries and there are lengthy periods when island formation shuts down. No discernible reflection of this behavior can be seen in the un-normalized reconnection rate, despite the behavior of the E²DR, which shows sharp reductions in length at a majority of the island emergence times. The normalized reconnection rate, however, does show local peaks following the emergence of most of the islands. These peaks are due to local reductions in the inflowing magnetic field strength at the position of the x-line, while a magnetic island remains nearby to it; they do not, in any way, reflect control of the reconnection rate due to changes in the geometry of the E²DR.

The conclusions of Hesse *et al.*[17] discussed above were limited to an analysis at a single point in an outflow jet produced in a periodic simulation. We have expanded that analysis to an entire outflow jet in this open-boundary simulation. We have found that, indeed, the electrons move with the magnetic field in the local Hall plane over the entire length of the outflow jet. Further, the inner boundary of this comoving region is at the outer boundary of the E²DR,

confirming the conjecture of Klimas *et al.*[12] mentioned above. Thus, for this jet, the entire outer EDR is a misnomer. In this region, the electrons are not outrunning the magnetic field, and the super-Alfvénic jet is a projection of the diamagnetic electron current sheet directed orthogonal to the local Hall plane but projected onto the simulation plane.

This paper is organized as follows: in Sec. II, we discuss the simulation setup. In Sec. III, we give an overview of the simulation under discussion, including a discussion of the relationship between the reconnection rate and the generation of magnetic islands, plus the long-time evolution of selected plasma parameters that enter the following discussion. In Sec. IV, we discuss the dimensions of the E^2DR, their relationships to other important length scales, and the relationship of the outflow boundaries of the E^2DR to the transition in the outflow jets to electron motion that is tied to the magnetic field in the local Hall frame. Section V contains a discussion of two empirical relations that yield excellent approximations to the reconnection rate and that depend on the dimensions of the E^2DR. In Sec. VI, we summarize our interpretation of the simulation results. The Appendix contains a brief discussion of some minor changes that have been made to the open-boundary simulation code since the publication of Klimas *et al.*[12]

II. SIMULATION SETUP

Except for the changes described above in the Introduction, plus some minor modifications given in this section and the Appendix, the setup for the simulation under discussion here is identical to that of Klimas *et al.*[12] To summarize: We have used the $2\frac{1}{2}$-dimensional electromagnetic PIC code described in Hesse *et al.*,[18] modified to incorporate the open inflow and outflow boundary conditions.[8] The electromagnetic fields are integrated implicitly to avoid the Courant constraint on the propagation of light waves.[18] Lengths are normalized with respect to the ion inertial length $d_i = c/\omega_i = c(e^2 n_0/\varepsilon_0 m_i)^{-1/2}$ using the initial current sheet density n_0, time is normalized to the inverse ion cyclotron frequency $\Omega_i = eB_0/m_i$ using the initial asymptotic magnetic field strength B_0, and velocities are normalized to the Alfvén speed V_{A0} computed using n_0 and B_0. The electric field is normalized by $V_{A0}B_0$. We use an (x, z) coordinate system with the x- and z-directions in the outflow and inflow directions, respectively. The system size is $L_x = 160d_i$ by $L_z = 80d_i$. The initial equilibrium configuration is a Harris sheet $B_x = \tanh(z/\lambda)$ with $\lambda = 0.5d_i$ and with an additional perturbation of the GEM reconnection challenge type,[19,20] leading to a 0.5% asymptotic perturbation field. No guide field is included.

The simulation discussed here was initialized with approximately 2.4×10^8 particles on a 1600×1200 grid in the $x \times z$ directions. The extra resolution in the z-direction, relative to the x-direction, ensures sufficient resolution of the electron current sheet and diffusion region details in the x-line neighborhood. Four particle species, two of ions and two of electrons, with mass ratio $m_i/m_e = 25$ were included. Background and foreground particle temperatures were initialized with $T_i = T_e = 0.25$. Using the asymptotic magnetic field

strength to define the electron cyclotron frequency $\Omega_e = eB_0/m_e$ and the current sheet density n_0 for the electron plasma frequency $\omega_e = (e^2 n_0/\varepsilon_0 m_e)^{1/2}$, we set $\omega_e/\Omega_e = 2$. This choice is equivalent to $V_{Ae0}/c = 1/2$, in which V_{Ae0} is the electron Alfvén speed, also based on the asymptotic magnetic field strength and the current sheet density. The possibility of errors in our results due to the presence of relativistic electrons in our non-relativistic simulation must be considered. We have confirmed that the electrons remain subluminal in the simulation discussed here and we rely on the implicit field pusher to remove the high frequency wave modes that might incorrectly interact with the high velocity electrons that are present. Additional simulations (not shown) with $\omega_e/\Omega_e = 2$ and $\omega_e/\Omega_e = 4$, albeit on smaller simulation grids, have shown no significant differences, thus confirming the reliability of the $\omega_e/\Omega_e = 2$ results. In units of n_0, the initial background particle density was set to 0.2 while, as discussed above, the density at the inflow boundaries was held close to the higher value 0.4 for all $t > 0$. Further details on the consequences of this choice are given in Sec. III B.

Charge conservation is guaranteed by an iterative application of a Langdon-Marder type correction[21] to the electric field at each time step. We set the boundary conditions on the electric field at the outflow boundaries by enforcing gradient free tangential components and adjusting the normal component to satisfy $\nabla \cdot \mathbf{E} = \rho$. At the inflow boundaries, we apply a gradient free boundary condition on the out-of-plane component, set the normal component to zero, and we leave the x-component unchanged from the previous time step. Then, the Langdon-Marder correction is applied to correct the electric field over the entire grid, including at the boundaries. We set the boundary conditions on the magnetic field at the outflow boundaries by enforcing gradient free tangential components and adjusting the normal component to satisfy $\nabla \cdot \mathbf{B} = \mathbf{0}$. The y-component of the boundary field is smoothed using simple box car smoothing with width one ion inertial length. At the inflow boundaries, we set the out-of-plane magnetic field component to zero. At each step in the iterative implicit field solver, we set the x-component of the magnetic field to satisfy $\nabla \times \mathbf{B} = \mathbf{j}$ and then the normal component to satisfy $\nabla \cdot \mathbf{B} = \mathbf{0}$. This totality of particle and field boundary conditions generally leads to stable, quiet solutions with no trace of charge buildup near the boundaries or anywhere else on the computational grid; the exception is the situation when an active x-line passes through an outflow boundary. In that case, the magnetic field boundary conditions have been modified temporarily over a small region near the x-line to prevent the development of a potentially unstable configuration, as explained in the Appendix. Further details are given in Klimas *et al.*[12]

III. SIMULATION OVERVIEW

In this section, we give a broad overview of the results of a single undriven reconnection simulation with no guide field and open inflow and outflow boundaries.

In our first attempts to achieve undriven simulations, we had simply placed a zero-gradient boundary condition on the out-of-plane electric field at the inflow boundaries.

Typically, with this approach, a major problem soon developed. With open outflow boundaries, drifting of the x-line toward one or the other of the outflow boundaries, depending on random fluctuations in the initial simulation state, is a familiar problem. With completely open inflow boundaries, the additional problem of the x-line drifting toward one or the other of the inflow boundaries arises. To avoid the requirement of a very large simulation domain to contain the x-line in the inflow directions, we have computed the average of the two out-of-plane electric field values just inside of the inflow boundaries at each x-position and then we have used this average for the boundary values at both inflow boundaries at that position. We have found that this technique successfully centers the x-line in the z-direction and, for a centered x-line, yields zero-gradient boundary conditions at both inflow boundaries.

Klimas et al.[12] never achieved quasi-steady state reconnection in their driven reconnection simulation. The inflow density slowly declined as the simulation proceeded and was still declining when the simulation was stopped. Serendipitously, this behavior led to the discovery of several correlative relationships in the simulation results that would not have been noticed otherwise. These relationships became some of the most important results of the paper.

Nevertheless, to overcome the problem of declining density, we have added a source of particles at the inflow boundaries that prevent the inflowing density from dropping below a predetermined value. For the simulation under discussion here, this inflow density was set above the initial background density. Consequently, at a point approximately 2/3 through the simulation, the plasma environment at the x-line changed considerably when inflowing plasma reached the x-line. In this way, two separate intervals of quasi-steady reconnection were achieved with a relatively rapid transition between the two, thereby demonstrating our ability to control the reconnection environment while simultaneously providing a more stringent test of the correlative relationships due to Klimas et al.[12]

A. Magnetic island generation and reconnection rate

Daughton et al.[4] and Karimabadi et al.[7] have found definite relationships between the emergence of magnetic islands and the reconnection rates in their undriven open-boundary simulations. In their driven open-boundary simulation, Klimas et al.[12] found an inconsistent relationship, with the emergence of some islands related to local peaks in the reconnection rate, the emergence of other islands unrelated to local peaks, and some local peaks in the reconnection rate unrelated to magnetic island emergence. In this section, we show that, for the undriven simulation under discussion here, there appears to be no relationship at all between magnetic island emergence and the reconnection electric field. This un-normalized reconnection rate remains fast throughout, changing significantly only when plasma from the inflow boundaries reaches the x-line.

We discuss a normalized reconnection rate in this section as well. We have used the magnetic field strength and electron density at symmetric positions just outside of the ion bounce region at the x-line to normalize the reconnection electric field by $V_{alf,in}B_{in}$, in which $V_{alf,in}$ is the Alfvén speed and B_{in} is the field strength, averaged between these two positions in the inflow regions. For this measure of the reconnection rate, we do find a relationship with magnetic islands, with the reconnection rate peaking for short periods following the appearance of most of the islands, particularly those that arise later in the simulation. This effect is due to a reduction in B_{in} at the x-line that is induced by the presence of the growing magnetic island, while it remains nearby to the x-line.

An overview of the dominant x-line propagation and associated magnetic island generation is provided in Figure 1. To find the evolving position $\left(x^*(t), z^*(t)\right)$ of the dominant neutral line, we search for the saddle point associated with it in the vector potential $A_y(x, z, t)$. There is generally more than one neutral line on the grid at any given time. The dominant neutral line is the one with the smallest value in $-A_y$ at its saddle point. We do not track the time evolution of the vector potential; we simply use it as a tool for plotting field lines or for finding the dominant neutral line. Thus, at any instant, we construct the vector potential by integrating $\nabla \times \mathbf{A} = \mathbf{B}$, first in the z-direction using $\partial A_y / \partial z = -B_x$ and setting $A_y(x, z_{\min}, t) = 0$ at some arbitrary x-position and then in the x-direction using $\partial A_y / \partial x = B_z$. The path of the dominant x-line is shown by the sequence of white crosses on the figure. The tendency of the x-line to drift toward an outflow boundary is apparent but the x-line remains far from a boundary in this simulation. Generally, we find that $z^*(t)$ remains close to but not exactly at zero in this open boundary simulation.

The color image of Figure 1 shows the evolution with time of $-A_y\left(x, z^*(t), t\right)$; in effect, we are taking a cut in the x-direction through the flux surface at the z-position of the x-line and showing how the flux surface on this cut evolves. This procedure produces a useful graphic for showing the evolution of the saddle containing the dominant x-line plus an overview in a compact format of the emergence and propagation of all of the magnetic islands produced in the simulation. The emergence of several islands out of the initial state can be seen at $t \approx 30$; these pass out of the simulation domain through the outflow boundaries by $t \approx 80 - 90$. A sequence of five major islands emerges during the interval starting at $t \approx 70$ and ending at $t \approx 140$, following which there is a long island-free interval. Notice that at $t \approx 230$ a final island emerges that is just leaving the x-line when the simulation ends. It is interesting that as each island moves away from its starting point, it drags the x-line with it for a brief period.

The black curve of Figure 2 shows the evolution of the reconnection rate as indicated by the strength of the out-of-plane electric field component at the position of the dominant x-line. As is often the case, there is an initial burst of reconnection followed by an undershoot, in this case, and then a slow recovery to an interval of quasi-steady reconnection. At $t \approx 180$ a relatively rapid decline begins, followed by a second interval of quasi-steady reconnection; this is the time at which the plasma from the inflow boundaries has reached the x-line. By the time at which the second interval

of quasi-steady reconnection is reached, almost all of the plasma of the initial state has been ejected and replaced. As noted above, five major islands emerged in the time interval 70–140. During this interval, the island emergence was too rapid and the reconnection field too noisy to say whether there was any relationship between them. Note, however, that the period of quasi-steady reconnection continues on well into the island-free interval without showing any significant change in rate. (There might be a slight shift upward but no significant change in noise level, both of which would be counter to the predictions of Daughton et al.[4] and Karimabadi et al.[7]) Notice also that the isolated island emergence at $t \approx 230$ shows no signature in the reconnection rate. Overall, there appears to be no evident relationship between island emergence and reconnection electric field in this simulation.

The red curve of Figure 2 shows the reconnection rate normalized by $V_{alf,in}B_{in}$ and the vertical bars at the top of the figure indicate the approximate times at which islands appeared in the simulation. Following the appearance of the pair of islands at $t \approx 75$ and $t \approx 86$ there is a weak indication of a possible peak in the normalized reconnection rate, although this appearance may simply reflect the evolution of the un-normalized reconnection rate, shifted upward somewhat. In contrast, the island at $t \approx 113$, the pair of islands at $t \approx 135$ and $t \approx 140$, and the island at $t \approx 230$ are all followed by significant bursts in the normalized reconnection rate. There is an additional short-lived peak in the rate at $t \approx 183$ that is unrelated to an accompanying island but is coincident with the arrival of plasma from the inflow boundaries, as evidenced by the onset of the decline in the reconnection rate at that time.

Figure 3 shows the evolution of the electron density and the magnetic field strength at the x-line just outside of the ion bounce region that we have used to compute $V_{alf,in}B_{in}$ for normalizing the reconnection rate; both the density and the field strength have been normalized by their initial values in this figure. The electron density shows a gradual decline, as in Klimas et al.,[12] until $t \approx 180$ when it jumps up to the level imposed by the inflow boundary conditions, where it remains until disturbed by the magnetic island emergence at $t \approx 230$.

Except for this last island, the density shows no response to the appearances of the islands. (Further details on the behavior of the electron density over the simulation domain are given in Sec. III B.) The field strength, however, shows significant reductions following the appearances of the magnetic islands at $t \approx 113$, $t \approx 135$, $t \approx 140$, and $t \approx 230$, plus at the time of the short-lived peak in the normalized reconnection rate at $t \approx 183$ that is coincident with the arrival of plasma from the inflow boundaries. The peaks in the normalized reconnection rate are directly due to the appearance of these reductions in B_{in}. The reductions related to magnetic islands are caused when one of the regions of reduced field strength that regularly precede and, in particular, follow the islands overlaps with the x-line while an island is still nearby to the x-line.

B. Evolution of selected plasma parameters

The rather abrupt reduction in reconnection rate at $t \approx 180$ shown in Figure 2 is due to the arrival at the x-line of plasma introduced at the inflow boundaries. Because of the additional particle sources that we have placed at the inflow boundaries, the state of this plasma is somewhat different from that of the original background plasma that had been flowing into the x-line neighborhood up until that time. As an example, Figure 4 shows the progression from inflow boundaries to x-line of the perturbation in electron density induced by our particle source at the inflow boundaries. The light gray curve shows that the density at the inflow boundaries was held at ≈ 0.4 over the entire simulation. The black curve shows the density at the x-line. At $t = 0$ that density was 1.2 (notice that the figure starts at $t = 20$). A vestige of the rapid reduction of the density at the x-line to the background level, 0.2, can be seen at the left edge of the figure. Following that reduction, all of the density measurements began a slow decline from the common initial background level until the inflowing plasma reached each measurement point, first nearer to the inflow boundaries and last at the x-line, at which point the density jumped up at each measurement point to a quasi-steady value for the remainder of the simulation. It is interesting that the final equilibrium state of
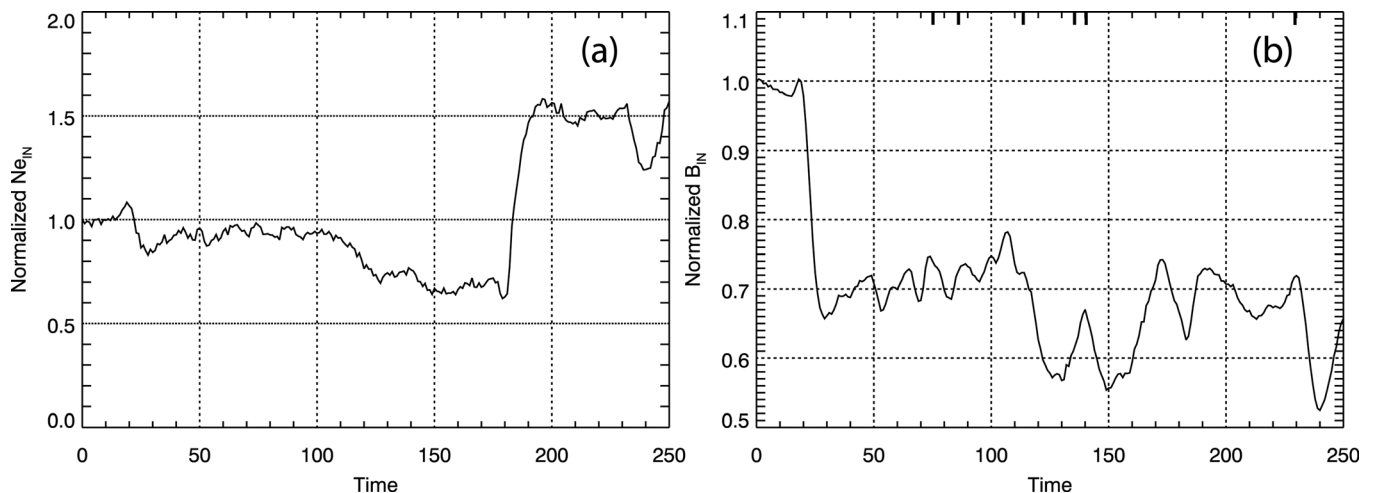

FIG. 3. (a) Inbound (see text) electron density normalized to initial value. (b) Inbound magnetic field strength normalized to initial value. Vertical bars at top of panel (b) show the approximate times at which magnetic islands appeared.
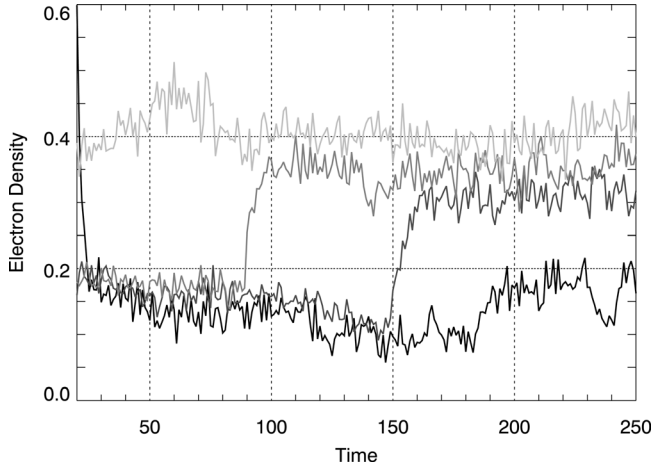
FIG. 4. The electron density at selected positions on the simulation domain. All curves are at the *x*-position of the dominant x-line. Averages of the values above and below the neutral plane are show where applicable. Notice that time starts at $t = 20$. Light gray: at the inflow boundaries. Gray: 1/3 of the distance inward from the inflow boundaries toward the neutral plane. Dark gray: 2/3 of the distance inward. Black: at the x-line.

the simulation required large-scale density gradients in the inflowing regions. The density dropout at $t \approx 230$ at the x-line is due to the emergence of a magnetic island at that time very near to the x-line. The ion density (not shown) did not share in this dropout. It appears that the forming island swept up electrons in it neighborhood but not ions, thus causing a temporary local charge imbalance in its surroundings.

Using the same format as in Figure 4, Figure 5 shows the evolution of the ion and electron temperatures at selected positions on the simulation domain. Both temperatures are computed from the traces of the respective pressure tensors. Ions at the x-line are heated significantly while elsewhere the ions experience a slow temperature decline from the initial value, 0.25. The high temperature at the x-line is due to the dominant P_{zz} contribution, which is a reflection of the ion bounce motion in the field reversal. The large P_{zz} balances the magnetic field pressure outside of the bounce region. At measurement points other than the x-line, the electrons experience the same slow temperature decline as the ions, and the

ion and electron temperatures remain approximately equal. The electrons at the x-line are heated somewhat initially (not shown), but then the electron temperature at the x-line declines slowly as well. The large drop in ion temperature starting at $t \approx 180$ is associated with the arrival of plasma from the inflow boundaries. The simultaneous rise in ion density, similar to that of the electrons in Figure 4, plus a temporary decline in magnetic field strength in the neighborhood of the x-line (not shown), all lead to pressure balance. At the end of the simulation, the ion temperature is approximately five times the electron temperature. While the electrons may have reached a quasi-steady state, the ion temperature at the x-line remains unsettled.

IV. E²DR DIMENSIONS

We define the extended electron diffusion region as that region surrounding the x-line in which the out-of-plane non-ideal electric field satisfies the condition

$$E_y' = -\left[\frac{1}{en_e}\nabla \cdot \mathbf{P}_e + \frac{m_e}{e}\mathbf{v}_e \cdot \nabla\mathbf{v}_e\right]_y > 0, \qquad (1)$$

in which a steady state is assumed. This E²DR definition contains two terms, the thermal term ($\nabla \cdot \mathbf{P}$) and the bulk inertia term ($\mathbf{v}_e \cdot \nabla\mathbf{v}_e$). In this section, we discuss the evolution with time of the length L of this region in the *x*-direction, its width d in the *z*-direction, and the relationships of these dimensions to other relevant physical length scales.

A. Length and width

We have measured the width and length of the E²DR over the course of the simulation under consideration. In the *x*-dimension, E_y' makes a clean transition from positive to negative as the distance from the neutral line increases in either direction. We have defined the full length L of the E²DR as the distance between these two points at which $E_y' = 0$. This is in agreement with the length of the inner region of Shay *et al.*[13] but differs from that of Karimabadi *et al.*,[7] who defined the length of the inner region as the distance between the maxima in the speeds of the outflow jets.
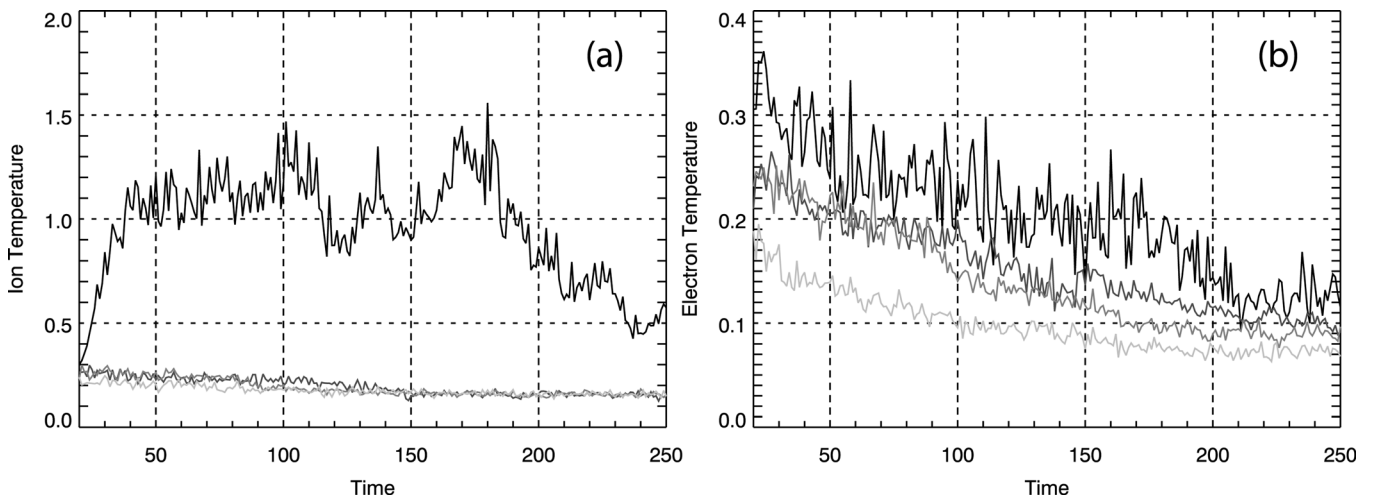

FIG. 5. (a) The ion temperature and (b) the electron temperature at selected positions on the simulation domain. Positions and gray scales are as in Figure 4.

In the z-dimension, E_y' approaches zero as the distance from the neutral line increases but the zero is masked by numerical noise that is superposed. We have chosen a threshold value that is as low as possible while still remaining above the noise level and have defined the full width d of the E^{2}DR as the distance between the two points at which E_y' equals this threshold value. Spatial averaging was necessary to obtain reliable results. Simple box-car averaging was applied over seven grid points in the x-direction and three in the z-direction.

Figure 6 shows the evolution of the length and width of the E^{2}DR over the course of the simulation under discussion. The width shows a general reduction in value in response to the inflowing plasma arrival at $t \approx 180$ but the length does not. As in the driven simulation of Klimas *et al.*,[12] the length appears approximately constant, with fluctuations superposed, except for isolated sharp reductions and slower recoveries at the emergence times of most of the islands. The reductions at $t \approx 110$ and $t \approx 230$ can be clearly identified with the emergence of islands shown in Figure 1. The reduction at $t \approx 140$ is related to one or both of two islands that emerge at about that time. We see no discernible relationship between these length reductions and the un-normalized reconnection rate shown in Figure 2.

B. E^{2}DR width compared to electron and ion bounce widths

We define the electron and ion bounce widths by finding those positions $z^* \pm \Delta z$, moving away from the x-line toward the inflow boundaries, at which the Larmor radius r_L in B_x is equal to the distance to the x-line; i.e., where

$$r_{L,e,i}(x^*, z^* \pm \Delta z) = \frac{m_{e,i} c v_{th,e,i}}{e|B_x(x^*, z^* \pm \Delta z)|} = \Delta z, \quad (2)$$

in which the excursions Δz in the two directions may not necessarily be equal. The bounce widths are defined as the distances between these two points for the electrons and the ions.

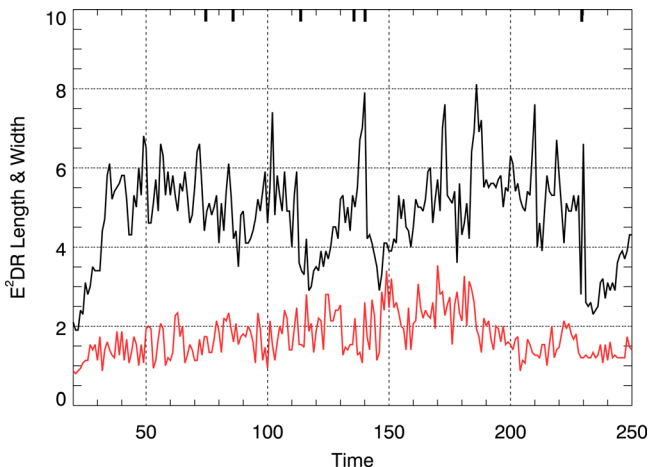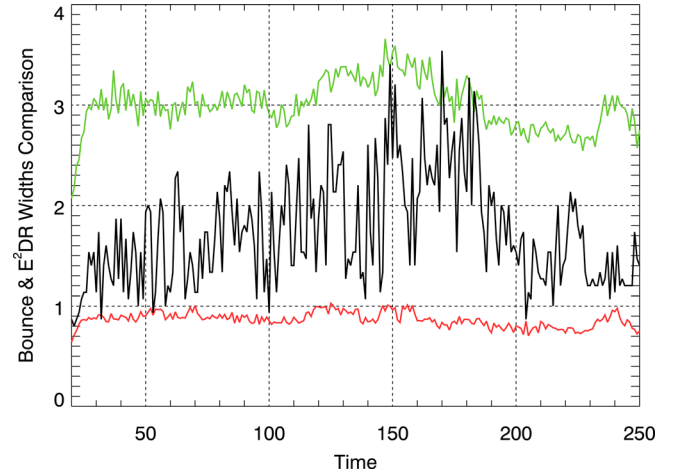Figure 7 shows a comparison of the E^{2}DR width d to the electron and ion bounce widths. As in Klimas *et al.*,[12] we

FIG. 7. Black: E^{2}DR width. Red (gray): electron bounce width. Green (light gray): ion bounce width.

find that the E^{2}DR width is larger than the electron bounce width; it does not appear that the electron bounce motion is decisive in setting the E^{2}DR width. In contrast to the driven simulation of Klimas *et al.*, however, we find that the E^{2}DR width appears smaller than, and unrelated to the ion bounce width. The long, gradual increase in d by almost a factor of two, over the interval $0 < t < 180$, is not reflected in the evolution of the ion bounce width. The ion bounce width peaks at $t \simeq 150$, earlier than d. While, following their respective peaks, both decline in value, the prolonged burst in d starting at $t \simeq 220$ is absent in the ion bounce width and the prolonged burst in the bounce width starting at $t \simeq 230$ is absent in the evolution of d. Thus, we conclude that the E^{2}DR width is an independent property of the electron dynamics and not just a reflection of the ion dynamics in the neighborhood of the x-line. Exactly what sets the width of the E^{2}DR, however, is unknown to us at present.

C. E^{2}DR length compared to electron turning length

Klimas *et al.*[12] have introduced a turning length scale, which is analogous to the bounce width scales discussed in Sec. IV B but oriented in the x-direction and calculated in the B_z field of the inner outflow jets. They showed that the boundaries of the E^{2}DR in the outflow directions are closely related to the turning points of that calculation and concluded, on that basis, that the boundaries marked the positions in the outflow jets where the electrons transition from unmagnetized to magnetized. Figure 8 shows a comparison of the length of the E^{2}DR with, as in Klimas *et al.*, $1.3\times$ the electron turning length scale. The number, 1.3, was chosen to produce the fit shown. We have no physical explanation for this number at this time. The figure reveals a very close relationship between the two length scales with the turning scale precisely reproducing the sharp reductions at island emergence times in the E^{2}DR length. This result confirms the results of Klimas *et al.* and shows that the boundaries, in the outflow directions, of the E^{2}DR mark the positions of the transition to magnetized electrons in both driven and undriven reconnection.

FIG. 6. Black: E^{2}DR length L. Red (gray): E^{2}DR width d. Vertical bars at top of figure show the approximate times at which magnetic islands appeared.
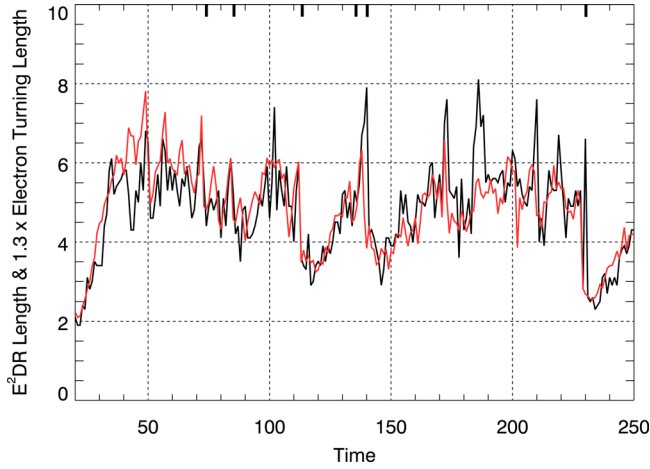
FIG. 8. Black: E^2DR length. Red (gray): $1.3\times$ electron turning length scale. Vertical bars at top of figure show the approximate times at which magnetic islands appeared.

D. Diamagnetic electron jet

Hesse *et al.*[17] have shown that at a point in the outflow jet of a periodic PIC reconnection simulation the electron nonideal electric field component that is orthogonal to the local Hall plane, $E'_{y'}$, is approximately zero, implying that the electrons are moving frozen to the magnetic field motion in this plane. This result is in conflict with the concept of an outer EDR containing a super-Alfvénic outflow jet. In this section, we extend the results of Hesse *et al.* by examining, in the local Hall plane, the velocity of the electrons relative to their drift velocity over the entire extent of an outflow jet.

Figure 9 shows the outflow jets that we have analyzed. The jet on the left of the x-line is impeded by a nearby island, and the results of our analysis for this jet are inconclusive. The jet on the right, which extends over approximately $20\, d_i$, provides reliable results that form the basis for our conclusions.

The first step in our analysis is to construct the local Hall plane at each x-position on the simulation domain. For this simulation, we have found that both B_x and B_y vary approximately linearly with z near the neutral plane. Thus, we have fit B_x and B_y linearly over ± 3 grid points in z at each position on the neutral plane (whose position in z does vary) and with

this fit have found the maximum and minimum values of these field components over the ± 3 grid point interval. Averaged field components, $B_x^{av}(x^*) = 0.5(|B_x^{max}| + |B_x^{min}|)$ and $B_y^{av}(x^*) = 0.5(|B_y^{max}| + |B_y^{min}|)$, were used to reconstruct the field in the neutral line neighborhood by applying appropriate positive or negative sign to the left or right of the x-line, above or below the neutral line. In this way, we obtained a smoothly varying field component basis for the local Hall plane.

Using normalized field components, $\boldsymbol{\beta} = \mathbf{B}^{av}/|\mathbf{B}^{av}|$, we have constructed the 2×2 projection operators $\mathbf{N} = \mathbf{I} - \mathbf{P}$ and $\mathbf{P} = \boldsymbol{\beta}\boldsymbol{\beta}$, in which $\mathbf{I}$ is the unit matrix. With these operators, we are able to find the components in the local Hall plane and orthogonal to the local Hall plane of any vector with x and y components. It is important to note that a fundamental assumption in this approach is that the transformation from the simulation plane to the local Hall plane consists of a rotation about the z-axis only.

With the drift velocity $\mathbf{v}_d = (\mathbf{E} \times \mathbf{B})/B^2$ and the electron velocity moment $\mathbf{v}_e$, the x and y components of the excess velocity $\mathbf{v}_e - \mathbf{v}_d$ are readily available in the neutral plane. The black curve in Figure 10 shows the x-component of this excess. Large excess speeds, of the order of two or more in the units of the Alfvén speed in use, are seen on both sides of the x-line, extending over the lengths of the outflow jets. In the averaged sense of the velocity moment, the electrons appear to be substantially outrunning the magnetic field in super-Alfvénic jets. The red curve, however, shows the result of projecting the excess velocity into the local Hall plane at every position along the neutral plane. To the right of the x-line at $x \approx 73$, the excess drift speed rapidly approaches zero and then fluctuates about that value over the total extent of the outflow jet. It appears that, in the local Hall plane, the electrons move with the magnetic field over the total extent of this jet. It should be noted that the transition into this "frozen in" motion takes place just outside of the vertical dashed and green (light gray) lines, which denote the positions of the electron turning point and the outflow
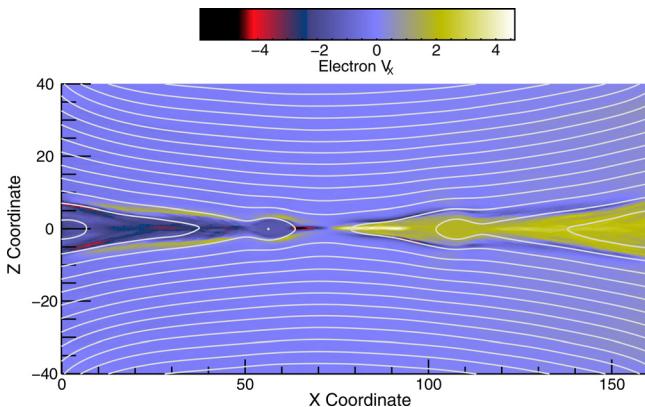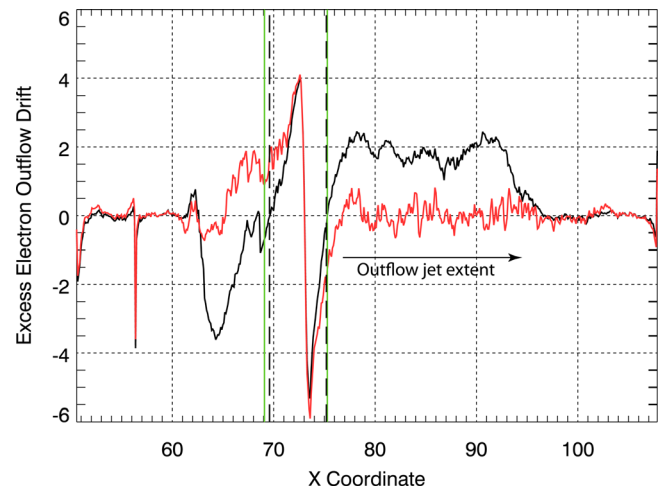

FIG. 9. Electron velocity component in x-direction with magnetic surface contours superposed at $t = 100$. All quantities time averaged over $1\,\Omega_i^{-1}$.

FIG. 10. Black: x-component of $\mathbf{v}_e - \mathbf{v}_d$ at the neutral plane. Red (gray): component in the local Hall plane of $\mathbf{v}_e - \mathbf{v}_d$ at the neutral plane. Black vertical dashed lines: electron turning points. Green (light grey) vertical lines: outflow boundaries of the E^2DR.

boundary of the E^{2}DR, respectively. Thus, for this jet, the conjecture of Klimas *et al.*[12] that the turning point and E^{2}DR outflow boundary positions together mark the inner boundary of the region of frozen in motion suggested by Hesse *et al.*[17] is correct.

The behavior of the red curve of Figure 10 on the left side of the x-line is similar to that on the right except that the transition to approximately zero excess drift speed takes place well outside of the turning point and E^{2}DR boundary positions and almost at the outer boundary of the jet. We assume that this difference in behavior is due to the presence of the nearby magnetic island that can be seen on Figure 9, the core of which lies at the position of the negative spikes in the black and red (gray) curves at $x \approx 56$.

V. RECONNECTION RATE

We have discovered two empirical expressions that involve the dimensions of the E^{2}DR and relate to the reconnection rate. These expressions are discussed in this section.

A. Aspect ratio

Using the full length L of the E^{2}DR in the outflow direction and the full width d in the inflow direction, we define the aspect ratio $R_A = d/L$. The black curve in Figure 11, reproduced from Figure 2, shows the normalized reconnection rate. Superposed, the red (gray) curve shows the fit given by the evolution of R_A. It can be seen that this fit reproduces most of the features of the reconnection rate, including the initial burst and relaxation starting at $t \approx 20$, the consequent gradual rise and saturation, the peaks following the emergence of the magnetic islands as well as the peak at $t \approx 180$ when the plasma from the inflow boundaries reaches the x-line, and, most notably, the steep reduction starting at that time.

We present this as an empirical result with no physical explanation at this time. Klimas *et al.*[12] presented a similarly successful fit of this sort. Thus, we can conclude that, whatever its basis, this relationship does not depend on the reconnection being driven or undriven.
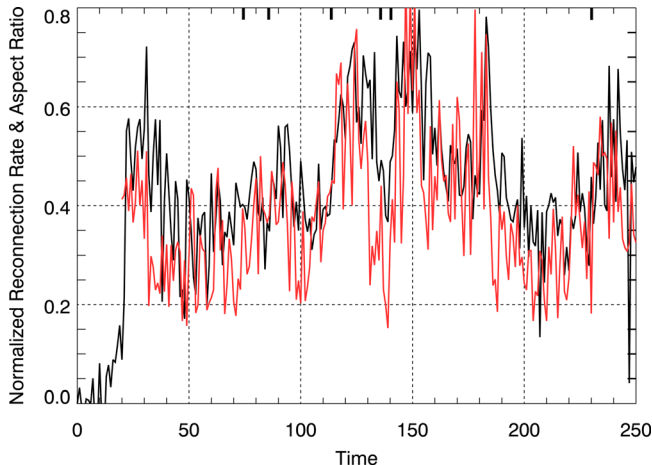
B. Ion temperature and E^{2}DR length

The black curve of Figure 12 shows the un-normalized reconnection rate while the red (gray) curve shows a fit produced by the simple expression

$$E_{y,rec} = T_i/L, \tag{3}$$

in which T_i is the ion temperature at the dominant x-line. Although the initial reconnection rate burst at $t \approx 20$ is not reproduced, the remainder of the reconnection rate evolution is surprisingly well fit.

In this case, Klimas *et al.*[12] have given a physical explanation based on the analyses of the non-gyrotropic components of the pressure tensor in Eq. (1) carried out by Hesse *et al.*[18] and Kuznetsova *et al.*[22] They have derived an approximate expression for the out-of-plane reconnection electric field given by

$$E_{y,rec} \simeq \frac{1}{e}\frac{\partial v_{xe}}{\partial x}\sqrt{2m_e T_e}, \tag{4}$$

in which the gradient in the electron velocity moment $\partial v_{xe}/\partial x$ and the electron temperature T_e are evaluated at the neutral line. Klimas *et al.* showed that if the electron parameters in Eq. (4), v_{xe}, m_e, and T_e, are replaced by the analogous ion parameters, the resulting expression also yields a very good fit to the measured reconnection rate (see their Figure 5). Klimas *et al.* further showed that the proportionality,

$$\frac{\partial v_{xi}}{\partial x} \propto \frac{v_{th,i}}{L}, \tag{5}$$

was very well satisfied for their driven simulation, thus leading to Eq. (3). This explanation applies as well to the undriven simulation under discussion here; however, the generality of this explanation is limited. A common feature of the results of both of these simulations is that the E^{2}DR length L fluctuates about an otherwise fixed value. In a follow up paper, in which we will discuss a group of driven simulations, we will see cases in which L exhibits long term
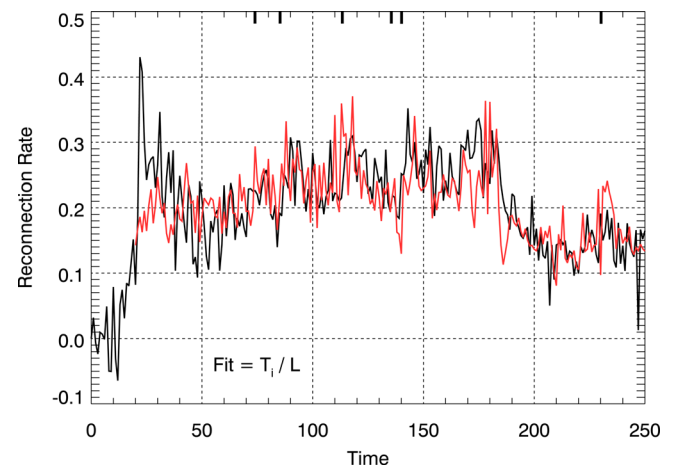

FIG. 11. Black: normalized reconnection rate. Red (gray): aspect ratio R_A. Vertical bars at top of figure show the approximate times at which magnetic islands appeared.

FIG. 12. Black: reconnection rate from out-of-plane electric field strength at x-line position. Red (gray): fit given by T_i/L. Vertical bars at top of figure show the approximate times at which magnetic islands appeared.

evolution. In those cases, this physical explanation for Eq. (3) will be shown to fail while Eq. (3) still remains an accurate approximation to the reconnection rate. A better understanding of the rationale for Eq. (3) is clearly necessary.

VI. DISCUSSION

We have discussed some results of an undriven, fully open-boundary PIC simulation of symmetric anti parallel reconnection.

We have shown that the simulation exhibits no relationship between magnetic island emergence and the unnormalized reconnection rate, as measured by the strength of the out-of-plane component of the electric field at the x-line position. This reconnection rate does drop dramatically when the plasma from the inflow boundaries reaches the x-line but no other tendency for it to decrease with increasing time has been found. We have shown that the normalized reconnection rate exhibits a significant response to the emergence of most of the magnetic islands and that the response in the form of localized peaks in the reconnection rate is due to dropouts in the inflowing magnetic field strength B_{in} at the dominant x-line. The dropouts are reflections of perturbations in the field strength produced by the islands, which overlap with the x-line when an island is nearby. While we have shown that the emergence of a magnetic island does lead to a reduction in the length of the E^2DR, the peaks in the normalized reconnection rate are unrelated to these reductions.

Our primary focus, in this paper, has been on the E^2DR. We have shown that its width, in the inflow directions, evolves considerably but remains between the electron and ion bounce widths and does not mirror the evolution of those length scales. We interpret this result as an indication that the E^2DR width represents the dynamics of the electrons in the diffusion region; it is not simply a reflection of the ion bounce dynamics, as had been concluded earlier.[12] We have shown that the E^2DR length, in the outflow directions, remains closely related to the turning length scale[12] in this undriven simulation. Thus, we have concluded that the outflow boundaries of the E^2DR mark the positions at which the electrons become magnetized in the outflow jets and we have shown one example in which such a boundary is at the inner edge of the so called super-Alfvénic outflow jet in the outer EDR. For this example, however, we have concluded that the entire outer EDR is a misnomer. In this region, the electrons are not outrunning the magnetic field, and the super-Alfvénic jet is actually a projection of the diamagnetic electron current sheet which is orthogonally directed to the local Hall plane but projected onto the simulation plane. While we feel that this is a convincing example, it is just one. Further confirmation of this point of view is desirable.

We have discussed two empirical relationships that yield excellent approximations to the reconnection rate while involving the dimensions of the E^2DR. For the first of these, the fit to the normalized reconnection rate given by the evolution of the aspect ratio R_A, we have provided no theoretical explanation at this time. For the second, the fit to the unnormalized reconnection rate given by T_i/L, we have provided an explanation, but we have also warned that it may

have limited validity. Further theoretical study of these relationships is necessary. We have not addressed the question of whether the electron dynamics of the E^2DR plays a role in governing the reconnection rate. However, it is clear from the performance of the empirical relationships that the E^2DR is intimately connected to the reconnection rate. On this basis, plus our rejection of the outer EDR concept, we suggest that it is the E^2DR that is the correct choice for the electron diffusion region for the case of two dimensional, anti parallel, symmetric reconnection. In contrast to the dissipation region,[15,16] a generalization of the diffusion region concept to guide field, and/or asymmetric reconnection is unavailable at this time. This is another issue that must be developed further.

ACKNOWLEDGMENTS

APPENDIX: MINOR CODE MODIFICATION

Without modification our open boundary conditions at the outflow boundaries are unstable following the passage of an active x-line that is associated with a moving magnetic island. What had been an outflow jet at the x-line then becomes an inflow jet at the boundary. The surrounding stretched magnetic field accelerates particles in this inflow jet toward the interior. Thus, when new particles are inserted at the boundary to maintain the gradient-free particle distribution at the boundary (see Klimas *et al.*[8]), they are inserted at a slightly higher inward speed. This process repeats to yield a faster and faster inward directed jet. To obtain the results discussed in this paper, we have modified the boundary conditions in a small region near $z = 0$ for the short time that is necessary to allow the passage of the x-line and its associated outflow jet to pass through the boundary. At the time at which the x-line reaches the boundary, we normally find $B_z \approx 0$ in a region near $z = 0$ on the boundary. Starting at that time, we begin holding $B_z = 0$ on the boundary in an appropriately small region surrounding $z = 0$. We choose a small enough region so that its presence is hidden from the rest of the simulation domain by the following magnetic island. This modification of the usual boundary condition is maintained until the core of the following island reaches the boundary; another time at which we should normally find $B_z = 0$ near $z = 0$ on the boundary. At that time, the modification is removed and the normal gradient free boundary condition is reinstated. We have found that this method works well to allow the smooth passage of the x-line and associated magnetic island through the boundary without disturbing the larger simulation domain.

[1]R. Horiuchi, W. B. Pei, and T. Sato, Earth, Planets Space **53**(6), 439–445 (2001).
[2]A. Ishizawa, R. Horiuchi, and H. Ohtani, Phys. Plasmas **11**(7), 3579–3585 (2004).
[3]A. Ishizawa and R. Horiuchi, Phys. Rev. Lett. **95**(4), 045003 (2005).
[4]W. Daughton, J. Scudder, and H. Karimabadi, Phys. Plasmas **13**(7), 072101 (2006).
[5]W. Daughton and H. Karimabadi, Phys. Plasmas **14**(7), 072303 (2007).

[6]A. V. Divin, M. I. Sitnov, M. Swisdak, and J. F. Drake, Geophys. Res. Lett. **34**(9), L09109, doi:10.1029/2007GL029292 (2007).

[7]H. Karimabadi, W. Daughton, and J. Scudder, Geophys. Res. Lett. **34**(13), L13104, doi:10.1029/2007GL030306 (2007).

[8]A. Klimas, M. Hesse, and S. Zenitani, Phys. Plasmas **15**(8), 082102 (2008).

[9]W. Wan and G. Lapenta, Phys. Plasmas **15**(10), 102302 (2008).

[10]W. Wan and G. Lapenta, Phys. Rev. Lett. **101**(1), 015001 (2008).

[11]H. Ohtani and R. Horiuchi, Plasma Fusion Res. **4**, 024 (2009).

[12]A. Klimas, M. Hesse, S. Zenitani, and M. Kuznetsova, Phys. Plasmas **17**, 112904 (2010).

[13]M. A. Shay, J. F. Drake, and M. Swisdak, Phys. Rev. Lett. **99**(15), 155002 (2007).

[14]J. F. Drake, M. A. Shay, and M. Swisdak, Phys. Plasmas **15**(4), 042306 (2008).

[15]S. Zenitani, M. Hesse, A. Klimas, C. Black, and M. Kuznetsova, Phys. Plasmas **18**(12), 122108 (2011).

[16]S. Zenitani, M. Hesse, A. Klimas, and M. Kuznetsova, Phys. Rev. Lett. **106**(19), 195003 (2011).

[17]M. Hesse, S. Zenitani, and A. Klimas, Phys. Plasmas **15**, 112102 (2008).

[18]M. Hesse, K. Schindler, J. Birn, and M. Kuznetsova, Phys. Plasmas **6**(5), 1781–1795 (1999).

[19]J. Birn, J. F. Drake, M. A. Shay, B. N. Rogers, R. E. Denton, M. Hesse, M. Kuznetsova, Z. W. Ma, A. Bhattacharjee, A. Otto, and P. L. Pritchett, J. Geophys. Res. **106**(A3), 3715–3719, doi:10.1029/1999JA900449 (2001).

[20]M. Hesse, J. Birn, and M. Kuznetsova, J. Geophys. Res. **106**(A3), 3721–3735, doi:10.1029/1999JA001002 (2001).

[21]A. B. Langdon, Comput. Phys. Commun. **70**(3), 447–450 (1992).

[22]M. M. Kuznetsova, M. Hesse, and D. Winske, J. Geophys. Res. **105**(A4), 7601–7616, doi:10.1029/1999JA900396 (2000).